

The sounds of failure: forecasting granular slip events with passive acoustic measurements

Theodore A. Brzinski^{1,2,*} & Karen E. Daniels¹

¹*Department of Physics and Astronomy, NC State University*

²*T.A.B. has joined the physics faculty at Haverford College since completing this work*

**Corresponding Author*

Granular materials, including those in geologic faults or concrete, can fail catastrophically through spontaneous, dramatic events like earthquakes or brittle fracture. However, in contrast to crystalline solids, disordered solids like granular materials cannot be described in terms of structural defects. Therefore, measurements and analytic models which forecast failure in this class of materials, while of both fundamental scientific and practical interest, remain elusive. Disordered solids ranging from numerical packings of spheres, to colloidal glasses, to granular materials have all been known to develop an excess of low-frequency vibrational modes as the confining pressure is reduced. Here, we report experiments on sheared granular materials in which we monitor the evolving density of excited modes via passive monitoring of acoustic emissions. Importantly, these results both provide a new interpretation of the changing state of the material on its approach to stick-slip failure, and can be used to forecast the rising risk.

The tools of statistical mechanics have shown great promise in describing the origins of rigidity in granular and other amorphous systems. The framework provided by the *jamming*

*transition*¹⁻³, while most-successfully applied to idealized, frictionless systems, has highlighted the extent to which such systems share certain properties: spatially and dynamically heterogeneous response to stress, structural disorder, and inhomogeneous force transmission. While this onset of rigidity shares features with standard second-order phase transitions, jamming is differentiated from other such transitions by its lack of a diverging structural length-scale. Meanwhile, the length and timescales which characterize the dynamics of these systems have been observed to diverge, indicating, that the transition may be purely dynamical in nature.⁴ Although jammed systems are not necessarily thermal, it has nonetheless been observed that the density of vibrational modes $D(\omega)$ remains an important descriptor of the state of the system. In particular, it is universally observed that an excess of low-frequency modes develops on approach to the jamming transition^{5,6} and the onset of plasticity⁷. Indeed, these excess low-frequency modes have been observed in experiments in colloidal systems^{8,9} as well as granular materials^{10,11}. One practical method for making such measurements has been to take advantage of the relationship between the particle velocity autocorrelation function and the density of vibrational modes.^{12,13}

Recent experiments on a quasi-2D packing of millimeter-scale (athermal) disks driven by a vibrating piston have used this relationship to establish a connection between acoustic modes and the jamming framework.¹¹ The key technique is to measure the velocity autocorrelation function

$$C_v(\tau) \equiv \frac{\sum v_k(t + \tau) v_k(t)}{\sum v_k(t) v_k(t)}, \quad (1)$$

for a set of $v_k(t)$ velocity timeseries measured using particle-scale piezoelectric sensors; the sums

over k covers all sensors in the system. The density of vibrational modes is then given by

$$D(\omega) = \int_0^\infty C_v(\tau) \cos(2\pi\omega\tau) d\tau. \quad (2)$$

The prior experiments confirmed the efficacy of this approach by recovering the expected Debye scaling for crystalline granular materials, as well as the expected excess of low- ω modes in both amorphous and crystalline systems as the confining pressure was reduced.¹¹ These results were robust even for measurements over a small subset of the particles.

These prior experiments and simulations tantalizingly suggest that information about the rigidity of a system might be encoded within $D(\omega)$ as the system evolves under external loading. $D(\omega)$ would a particularly attractive metric since the passive recording of acoustic emissions provides a non-invasive method of reporting changes in the state of the system. For example, embedded sensors have long been used for non-destructive evaluation of engineered structures^{14,15}, and have also successfully identified precursors in volcanic systems¹⁶. A key advantage of acoustic emissions methods is that they do not require visual access to the system. Our experiments are inspired by prior work on slowly-loaded granular materials, from which it is known that (1) particle-scale rearrangements both precede and follow failure events¹⁷, and (2) acoustic emissions and microslips show an exponential increase in their rate of occurrence leading up to a failure event^{18,19}. Here, we measure the acoustic emissions during the the lead-up to failure, and associate changes in the observed $D(\omega)$ with the approach to failure. In doing so, we provide a new physical interpretation for the ongoing changes in the state of the system which will improve the utility of acoustic monitoring as a forecasting method. Unlike spectral power measurements, which capture the distribution of acoustic power among modes of different frequencies, the approach we

introduce is effectively a measurement of the number of modes which are excited, regardless of the excitation amplitude.

Our experiment comprises an annulus filled with a single layers of disk-shaped particles, sheared via a torsion spring to produce intermittent stick-slip failure events (see Fig. 1a-c). We measure the driving torque (**d**) and acoustic emissions (**e**) of the system continuously (see *Methods* section for details). Rather than focusing on the high-amplitude emissions that accompany each slip event, we instead investigate the low-amplitude emissions during the largely quiescent periods between these slips. We find that these emissions are characterized by systematic changes in the density of excited modes, $D_{\text{ex}}(f)$.

Below, we test the viability of this approach for forecasting the catastrophic material failure of the granular material. First, we segment the data into 1 second increments, each centered at time $t - t_i$ where t_i is the time of an observed slip. We then calculate the granular density of *excited* vibrational modes $D_{\text{ex}}(f; t - t_i)$ for each segment, following Eqs.1-2. During these periods, the acoustics emissions arise from both particle-scale rearrangements, and noise associated with the shear driving. We find that the mean, variance and kurtosis of f , measured from $D_{\text{ex}}(f; t - t_i)$, all evolve monotonically during quiescent periods and then change discontinuously in response to a slip. This behavior suggests useful and potentially predictive information may be encoded in the granular density of excited vibrational modes. Furthermore, we find that single-sensor acoustic measurements of D_{ex} during individual slips exhibit statistically significant discontinuities in $\langle f \rangle$ for 43% of measurements, in the variance for 38% of measurements and in the kurtosis for 54% of

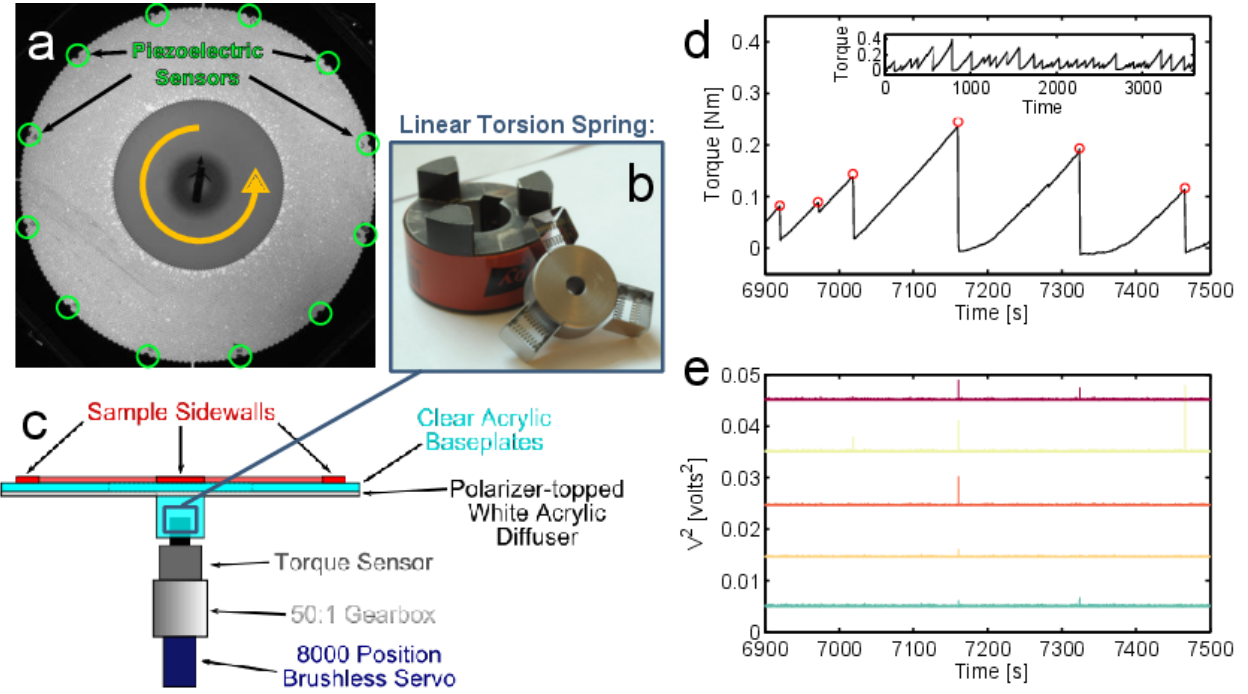


Figure 1: (a) Top view of the annular shear cell, with 12 piezoelectric sensors indicated in green. The shear direction is indicated on the moving (inner) wall. (b) Driveshaft coupling with custom torsion spring; compression of the internal coil springs provides a Hookean response. (c) Schematic side view illustrating the details of the drive system. A Parker Motion brushless servo motor drives the rotation of the inner wall and the resulting torque is measured by a Cooper Instruments torque sensor. (d) Sample torque timeseries over the course of 10 minutes and (inset) 1 hour. Red circles identify times at which slips were identified as sudden drops in torque. (e) Sample measurements of the voltage squared, $V^2(t)$, measured for 5 piezoelectric sensors, vertically offset for clarity and plotted on the same time axis as d. Each recorded acoustic emission appears as a voltage spike.

measurements. These results show promise for a new path towards passive, non-destructive testing and predictive monitoring of granular materials.

Results

Torque measurements: Due to the slow loading and fast unloading of the torsional spring, the torque on the granular material (provided by the rough inner wall) exhibits a repeating sawtooth shape characteristic of stick-slip motion (see Fig. 1d). The loading phase corresponds to the compression of the torsional spring, and when the applied torque surpasses the strength of the granular material, failure occurs. We perform automated detection of the slip events by identifying negative peaks in the derivative of the torque timeseries, and finding the nearest zero-crossings before/after these peaks. These identifications are shown as the open red circles. The full dataset of 1165 slip events are aperiodic and span a broad range of torque and time scales (see inset), indicating strong heterogeneity in the material strength and degree of deformation. Despite the spatiotemporal heterogeneity, the slip durations exhibit a relatively narrow duration distribution with a mean of 0.65 ± 0.14 s. This slipping time scale is well-separated from the inter-slip (quiescent) timescale, of which 887, more than 80% of the quiescent periods, have a duration of 30 seconds or longer. We focus our analysis on this subset of 887 slips to isolate the effects of individual slip events.

Acoustic measurements: The voltage produced across a piezoelectric material is linearly proportional to the applied stress; this value is also proportional to the acceleration of the particle in which such a sensor is embedded. Therefore, we integrate the voltage timeseries in order to obtain

the velocity timeseries $v(t)$ in arbitrary units. An illustration of the typical intermittency of these emissions is provided in Fig. 1e; each trace is the recorded voltage from one of 5 piezoelectric sensors, squared for visual clarity. The typical RMS voltage during quiescent periods (without large torque drops) is 2.0 mV (consistent with the 1.34 mV noise floor of our data acquisition hardware), while emission events can produce spikes as much as 3 orders of magnitude higher. The RMS Voltage only during slips is 5.8 mV. This includes null measurements. Excluding measurements where V was within 2σ of the quiescent RMS value, the slip RMS voltage climbs to 17 mV. We observe that the largest acoustic emissions always coincide with a torque drop (slip event). Importantly, the converse is not the case: not every slip produces a voltage spike in every sensor. This arises because the force chains cause the spatial variations in acoustic transmission to be highly heterogeneous²⁰.

As a control, we examine the power spectrum density $\text{PSD}(f; t - t_i)$ (spectrogram) for four representative slips, following a method typical of acoustic emissions experiments (see Fig. 2). For the chosen piezoelectric sensor, we divide the voltage timeseries into 1 s intervals centered around the detected slip; 61 of these are shown in each sample spectrogram. In all four spectrograms (b), the most dominant feature is the broad-spectrum emission centered at each slip. In addition, we observe several persistent frequencies which appear as horizontal lines. While the 60 Hz peak is of electronic origin, the others are likely due to persistent sources of acoustic noise such as from the drive system or building noise. Beyond that, there are only small background fluctuations which don't appear to change in magnitude or character either leading up to the slip or in response to it.

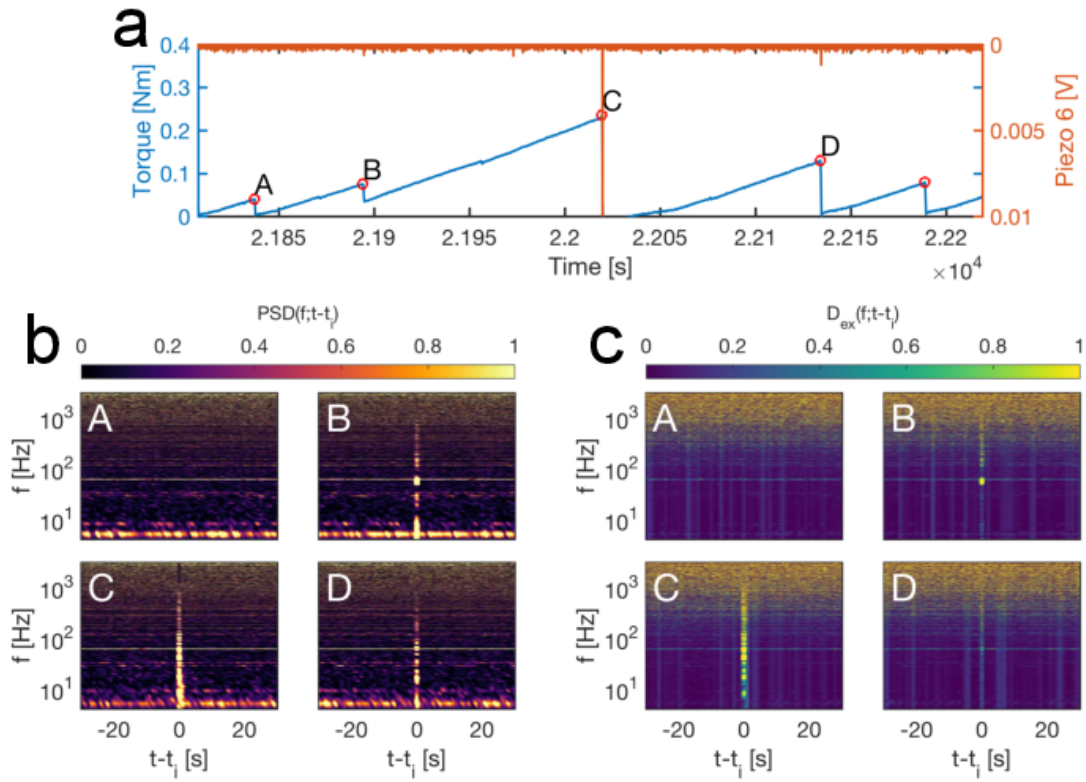


Figure 2: **(a)** Approximately 400 s of torque (blue) and voltage measurements (red) from one of twelve piezoelectric sensors, including 5 slips labelled with red circles. Sample **(b)** spectrograms showing the power spectrum density $PSD(f; t - t_i)$ and **(c)** modograms showing the density of excited modes $D_{ex}(f; t - t_i)$, both for an interval of ± 30 s centered on each of the four labeled slips (A-D).

Examining the density of excited states, $D_{\text{ex}}(f; t - t_i)$, proceeds in an analogous way, and the same representative samples (modograms) are shown in Fig. 2c. For each 1 s window, we calculate $D_{\text{ex}}(f)$ via the velocity autocorrelation function $C_v(\tau)$ (Eq. 1) and its transform (Eq. 2).^{12,13} A brief outline of this calculation, including sample data, is provided in Fig. ?? of the Methods. As also observed in the spectrograms, one prominent feature is that a broad range of modes is excited during each slip ($t - t_i = 0$). However, unlike the spectrograms, similar increases in excited modes are also observed at times before and after the slips; these features are visible as bright vertical bands. We will examine these in more detail below, and how they are associated with a small but important trend by which the modal density becomes non-uniform during the build-up to and recovery from each slip event. In addition, we observe that the overall density of excited modes appears to be relatively flat over nearly 3 decades (Hz to kHz), rising only at the highest frequencies in this range. Finally, the same noise peaks are present in both the spectrogram and the modogram, and will be filtered out in the later stages of analysis.

Analysis We begin by focusing on the vertical bands visible in Fig. 2c. Each of these bands represents a time at which a single piezoelectric sensor was able to (briefly) detect an increase in the number of excited vibrational modes over a broad range of frequencies. Some of these vertical bands correspond to global slip events ($t - t_i = 0$), but most are detected due to local rearrangements which happened to occur close to a particular sensor. The local nature of these detections is reinforced by the observation that modograms from different sensors do not necessarily record increases at coincident times (as also seen in Fig. 1e). This again reflects the spatial heterogeneity of sound propagation in the granular material. The ability to measure the $D_{\text{ex}}(f; t - t_i)$ from either

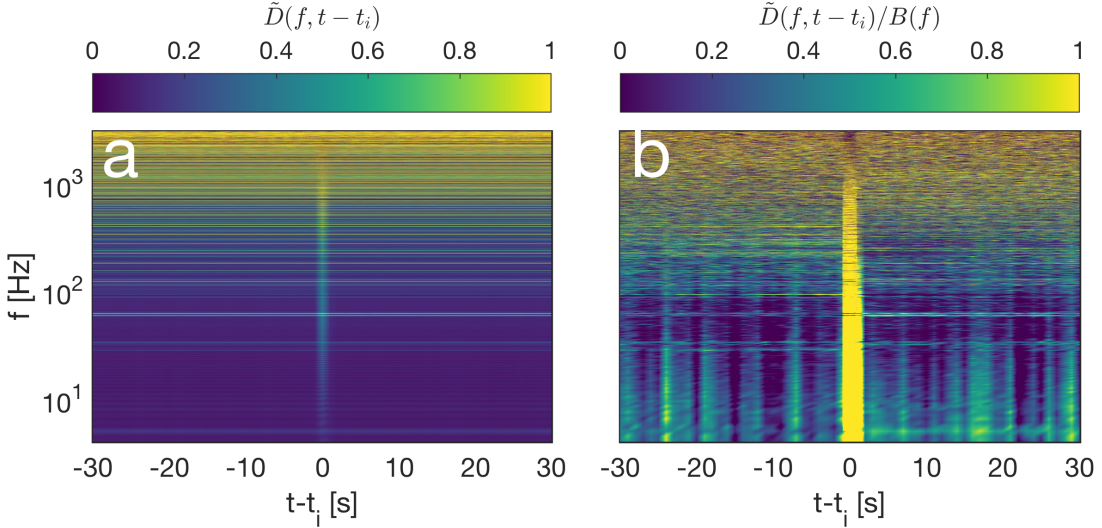


Figure 3: Average modograms $\tilde{D}_{\text{ex}}(f; t - t_i)$, taken over 887 slips and 12 sensors, shown **(a)** as raw data and **(b)** with the frequency-background $B(f)$ divided out.

low- or high-amplitude slip events is crucially-important to this method. While the low-amplitude events are too small to cause a global slip event, some of them are nonetheless large enough to be detected as they travel through the granular material and thereby leave a record of the state of the material. As we shall see below, the information they transmit reveals the changing state of the materials.

To reveal these small features, we can remove the background signal caused by the electronic/physical resonances. To do this, we construct the average modogram $\tilde{D}_{\text{ex}}(f; t - t_i) \equiv \langle D_{\text{ex}}(f; t - t_i) \rangle_{i,k}$, where i are the 887 detected slips separated by at least 30 s from the adjacent slips, and k are the 12 sensors. This average modogram is shown in Fig. 3a. To remove the persistent horizontal streaks (electronic/physical resonances), we calculate a background signal $B(f) = \langle \tilde{D}_{\text{ex}}(f; t - t_i) \rangle_{t \neq t_i}$, which we divide from $\tilde{D}_{\text{ex}}(f; t - t_i)$ to obtain the rescaled modogram

shown in Fig. 3**b**.

This average modogram exhibits features similar to the fluctuations observed in Fig. 2, but now the vertical streaks result from the average behavior over *many* slips and sensors. The remaining heterogeneity indicates that 887 slips was an insufficient quantity of data to eliminate the temporal heterogeneity associated with localized plasticity. Within this noisy signal, however, there emerge clear differences between the pre- and post-slip portions of this modogram. We examine these below, using raw $\tilde{D}_{\text{ex}}(f; t - t_i)$ (background not removed).

To quantify these changes, we plot the four moments of the slip- and sensor-averaged $\tilde{D}_{\text{ex}}(f; t - t_i)$, calculated at fixed times pre- and post-slip, as shown in Fig. 4. We find that the mean frequency (a) gradually grows during the pre-slip phase, and then suddenly decreases from 1.60 to 1.59 kHz (less than 1%) in response to slips. We also observe similarly clear, but still small, signals in the higher central moments of \tilde{D}_{ex} : a small increase in the variance, a weak minima in skewness and a 1% drop in the kurtosis (panels **b-d**, respectively). These changes are consistent with a broadening of $\tilde{D}_{\text{ex}}(f)$ on the approach to failure, with additional modes arising at lower-frequencies. Furthermore, since the internal stress in the granular material is lower after a slip (see Fig. 1**d**), these observations are consistent with the observation that excess low-frequency modes emerge at smaller confining pressures in acoustically-driven granular materials.¹¹

The values of the two higher-order moments are helpful in understanding the shape of \tilde{D}_{ex} . Recall that the skewness is a measure of the asymmetry of a distribution. Here, we find a skewness of ≈ 0.66 , which means low frequency modes are more common than high-frequency modes.

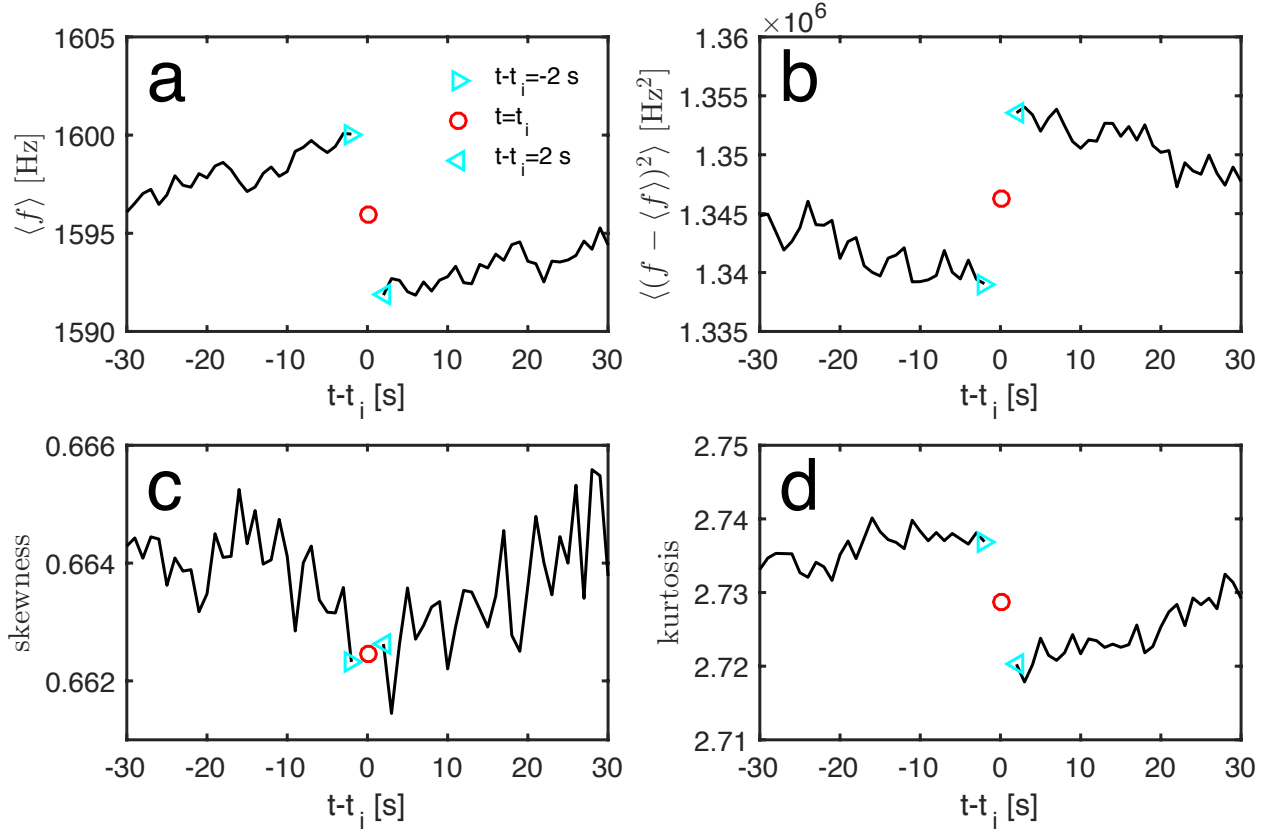


Figure 4: The four moments of $\tilde{D}_{\text{ex}}(f; t - t_i)$, calculated at fixed times pre- and post-slip: **(a)** mean frequency, **(b)** variance, **(c)** skewness, and **(d)** kurtosis. The red ‘o’ indicates the time of the slip (datapoint omitted for clarity). The right- and left-pointing cyan triangles indicate the values immediately before and after the slip.

Also recall that the kurtosis is a measure of the prevalence of extreme fluctuations where a larger kurtosis indicates fewer extreme modes. A normal distribution has a kurtosis of 3, so \tilde{D}_{ex} is neither particularly heavy- nor weak-tailed.

Finally, we consider D_{ex} as a possible metric for characterizing single-slip, single-sensor measurements. In Fig. 5 we examine a characteristic example for a period centered on a single slip **(a)**. Panels **(b,c)** present $\langle f \rangle$ and $\langle (f - \langle f \rangle)^2 \rangle$ of the excited modes, calculated based on a single sensor. To highlight the stepwise change in this noisy data, we additionally plot the mean $\pm 2\sigma$ as horizontal lines during the pre- and post-phases. Like the ensemble-averaged data (Fig. 4), we observe a significant drop in $\langle f \rangle$ coincident with the slip at $t = t_i$ accompanied by rise in the variance.

We perform this same analysis for all slips that are well-separated in time, for all 12 piezos, for a 10644 sets of statistics of the type shown in Fig. 5. Overall, we find that single sensor measurements are consistent with the average trends depicted in Fig. 4: 34% of measurements exhibit statistically significant drops in $\langle f \rangle$ (as opposed to 9% with significant rises) and 30% of measurements exhibit significant rises in $\langle (f - \langle f \rangle)^2 \rangle$ (8% with drops). The kurtosis exhibits statistically significant changes 54% of the time. While this is a higher rate of discontinuity than in either $\langle f \rangle$ or $\langle (f - \langle f \rangle)^2 \rangle$, only 35% of measurements exhibited drops consistent with Fig. 4 while 19% exhibited rises. These statistics are summarized in Table 1. Importantly, some slips will produce a detectable signal in $\langle f \rangle$ and the other metrics for only one or a subset of sensors. Moreover, some slips produce no signal at any sensor due to the dissipative nature of the system

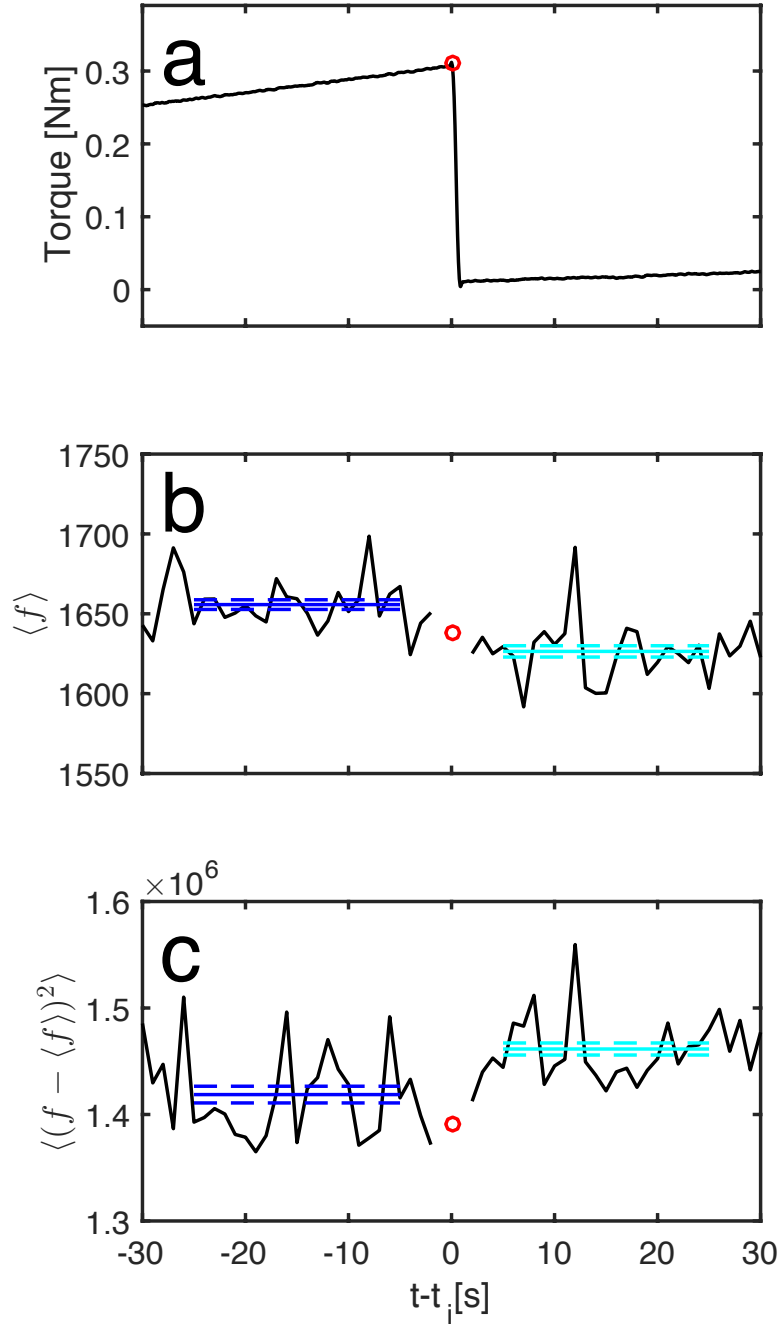


Figure 5: **(a)** Torque timeseries, measured at the inner wall, for a ± 30 s interval centered on a single slip event. **(b)** $\langle f \rangle$ and **(c)** $\langle (f - \langle f \rangle)^2 \rangle$ for $D_{\text{ex}}(f; t - t_i)$ for the same slip, measured by a single sensor. The solid blue and cyan lines show the mean values for the first and last 28 seconds respectively, and dashed lines show the 95%-confidence in these means.

	Significant Rise	Significant Drop	Null
mean	9%	34%	57%
variance	30%	8%	62%
kurtosis	19%	35%	36%

Table 1: The success rate for single-sensor measurements for which we observed statistically significant discontinuities in the mean, variance and kurtosis in f for D_{ex} at a time coincident with a slip. Boldface values are those that match the sign of the average changes in Fig. 4.

and because the 12 sensors, each approximately 5 mm wide, cover less than than 1% of the length of the perimeter.

Discussion

Assessing the internal stress state of a granular system is notoriously difficult: photoelastic, optical, and tomographic techniques^{21–23} require specialized materials and/or slow scanning times in order to make quantitative measurements of internal forces. We have found that the density of excited vibrational modes $D_{\text{ex}}(f)$ appears to provide a new technique for reporting the internal stress in the system which does not require optical access, and can be applied to 3D systems without requiring slow scanning. Importantly, this method does not require acoustically-driving the system, which risks triggering a failure in materials near threshold, and should work on any material composition. Furthermore, this new analysis is largely independent of the details of the sensor mechanism, so a clear next step is to test the approach with publicly available seismic data or data

collected with commercially available sensors such as those described in Ref. ¹⁵. Future work will also uncover whether the current need for averaging, either via extensive sensor coverage or by ensemble-averaging, can be mitigated through improved sensors.

The measurements we present here represent an important step in connecting passive acoustic measurements directly to the state of the material. While acoustic emissions have previously been known coincide with the failure of granular media, the method presented here provides a new capability: assessment of progress of a system en route to failure. The shift observed in moments of the occupancy of vibrational modes is consistent with observations that granular systems under less stress exhibit an excess of floppy, low-frequency modes¹¹, and can be connected more broadly to similar observations in jammed solids as the volume fraction is reduced ^{8,9,24} and as shear progresses ²⁵. Our results indicate promise for predictive forecasting in systems with more complete sensor coverage, where passive measurements may more completely reveal the features of the density of vibrational modes. These techniques also provide a route for improved characterization of the vibrational properties of disordered materials.

Methods

Granular material The material used in the experiment comprises a 60:40 mixture of approximately 8000 circular and elliptical disks; the circular grains are 5.6 mm in diameter, while the axes of the elliptic grains are 4.9 and 6.9 mm. All grains are 3.2 mm tall, and are milled from PhotoStress Plus PS-3 polymer from the Vishay Measurements Group; the bulk elastic modulus of 0.21 GPa. The sizes are chosen so that circular and elliptic particles occupy approximately the

same area, and the mixture of shapes is used to prevent crystallization. The material is confined in a 32-grain-diameter gap between an inner wall of diameter 30.5 cm with 159 regularly spaced semicircular cutouts of diameter 4.6 mm, and an outer wall of diameter 66.75 cm with 45 regularly spaced semicircular cutouts of diameter 9 mm. The preparation protocol is to place handfuls of ~ 50 particles at a time onto the bottom plate after determining the particle count by mass. As the material approaches full coverage of the experimental cell, the final grains are added by sliding them into the sample from the sidewalls. Once all grains are placed, a top-plate is placed over the packing (with a gap of ≈ 4 mm). This preparation results in a packing that, under shear stress, produces typical stick-slip motion.

Shear procedure The center wall is fastened to a 30.5 cm diameter acrylic turntable, which is connected by a modified Lovejoy coupling to the driveshaft of a brushless servo motor (Parker Bayside BE231FJ-NLCN with PV90FB 50:1 gearbox). The driveshaft coupling is modified to serve as a custom torsion spring with a spring-rate of 0.85 Nm/radian and a maximum compression of 26° , corresponding to a torque of 0.39 Nm (see Fig. 1b). The motor turns at a constant rate of 1 rotation per hour, and a Cooper Instruments torque sensor in line with the driveshaft measures the total torque exerted on the inner wall. The resulting stick-slip motion of the inner wall is characterized by periods of monotonically increasing torque separated by sudden, step-like slips. Empirically, the initial frequency of these slips is around 2 slips/minute and quickly drops to below 1 slip/minute over the course of ≈ 2500 s. After this initial transient, the frequency of slips remains close to 1 slip/minute. Before taking data, the system is sheared sufficiently to remove this initial transient. The data presented here was collected over the course of approximately 23 hours.

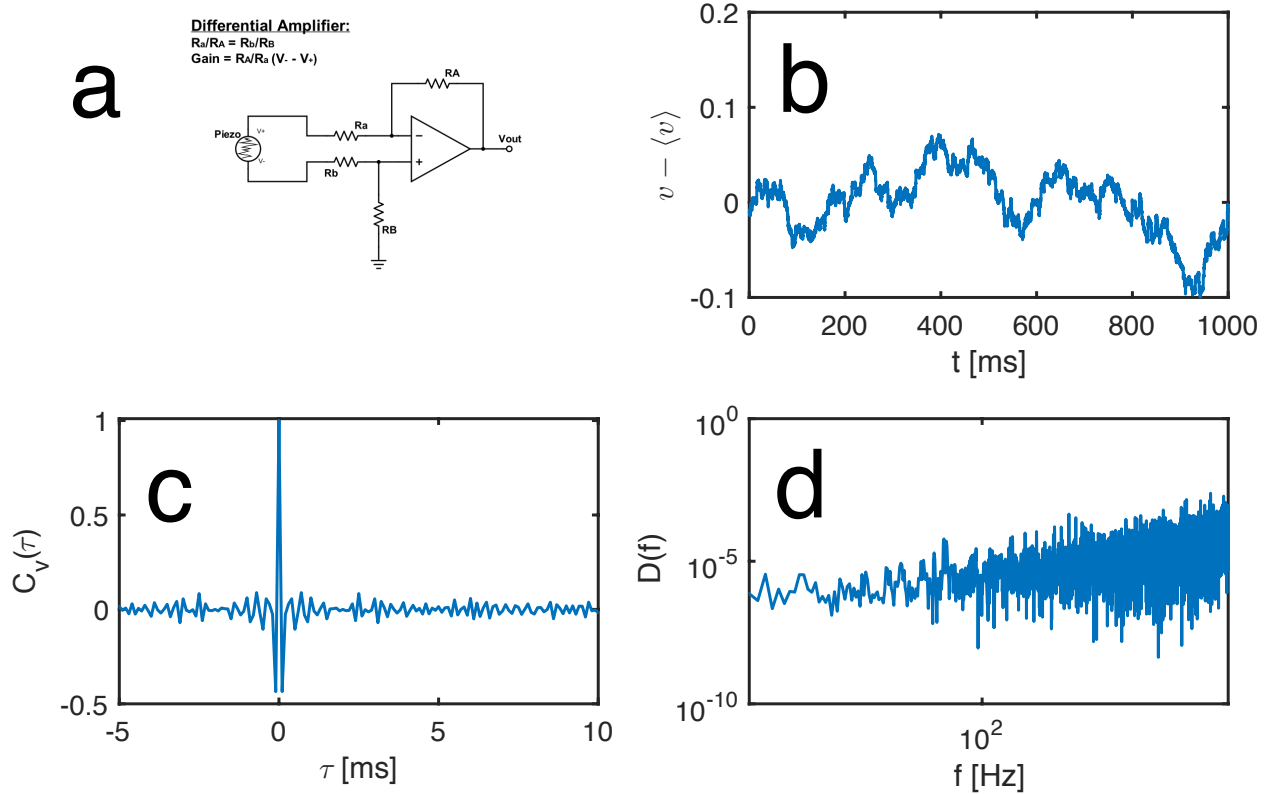


Figure 6: (a) A schematic of the differential amplifier. (b) The velocity (in arbitrary units) calculated from the voltage of a single piezoelectric sensor signal during a period of quiescence. (c) The corresponding velocity autocorrelation function $C_v(\tau)$ plotted as a function of lag time, calculated according to Eq. 1. The signal decorrelates on the order of milliseconds. (d) The density of excited vibrational modes calculated from C_v , according to Eq. 2.

Acoustic measurements Acoustic emissions are characterized by measuring the voltage across bare piezoelectric ceramic elements^{11,20} embedded 3.1 mm from the edge of the outer wall. These custom acoustic sensors are unidirectional, with the measurement axis oriented radially. The voltages are amplified by a simple linear differential amplifier (see Fig. 6(a)), and sampled with a National Instruments Data Acquisition card (PXIE-6368) at a rate of 10 kHz. The amplifier was designed to have high input and low output impedances. The most important feature for our application is a high common-mode rejection: only the voltage difference across the piezoelectric sensor is amplified. This proved especially important in dealing with electromagnetic noise produced by the servo motor.

In order to calculate $D_{\text{ex}}(f; t - t_i)$ and $\text{PSD}(f; t - t_i)$ from the piezoelectric voltage, the data is segmented in 1 s increments. Because piezoelectric materials have a linear response, fluctuations in the measured voltage are proportional to the force between the piezoelectric sensor and grains within the packing. Integrating the voltage thus gives a value proportional to the instantaneous velocity of grains in contact with sensor. A calibrated velocity value is unnecessary since all values are normalized.

The steps taken in calculating $D_{\text{ex}}(f; t - t_i)$ for a 1 second data segment are shown explicitly in Fig. 6(b-d). This segment is not coincident with a slip. The measured piezoelectric voltage (which is proportional to the pressure on the sensor) is integrated to get a velocity in arbitrary units (a). This quantity is then used to calculate $C_v(\tau)$ according to Eq. 1. The central peak in C_v is plotted in Fig. 6(b). Finally, (c) we define D_{ex} as the real part of the Fourier transform of C_v .

1. Liu, A. J. & Nagel, S. R. *Jamming and Rheology: Constrained Dynamics on Microscopic and Macroscopic Scales* (CRC Press, 2001).
2. Liu, A. J. & Nagel, S. R. The Jamming Transition and the Marginally Jammed Solid. *Annual Review of Condensed Matter Physics* **1**, 347–369 (2010).
3. van Hecke, M. Jamming of soft particles: geometry, mechanics, scaling and isostaticity. *J. Phys.: Cond. Matt.* **22**, 33101 (2010).
4. Berthier, L., Biroli, G., Bouchaud, J.-P., Cipelletti, L. & van Saarloos, W. *Dynamical Heterogeneities in Glasses, Colloids, and Granular Media (International Series of Monographs on Physics)* (Oxford University Press, 2011).
5. O’Hern, C. S., Silbert, L. E., Liu, A. J. & Nagel, S. R. Jamming at zero temperature and zero applied stress: The epitome of disorder. *Phys. Rev. E* **68** (2003).
6. Wyart, M. On The Rigidity Of Amorphous Solids. *Annales De Physique* **30**, 1 (2005).
7. Tanguy, A., Mantisi, B. & Tsamados, M. Vibrational modes as a predictor for plasticity in a model glass. *Europhysics Letters* **90**, 16004 (2010).
8. Ghosh, A., Chikkadi, V. K., Schall, P., Kurchan, J. & Bonn, D. Density of states of colloidal glasses. *Phys. Rev. Lett.* **104**, 248305 (2010).
9. Chen, K. *et al.* Low-frequency vibrations of soft colloidal glasses. *Phys. Rev. Lett.* **105**, 025501 (2010).

10. Brito, C., Dauchot, O., Biroli, G. & Bouchaud, J.-P. Elementary excitation modes in a granular glass above jamming. *Soft Matter* **6**, 3013 (2010).
11. Owens, E. T. & Daniels, K. E. Acoustic measurement of a granular density of modes. *Soft Matter* **9**, 1214–1219 (2013).
12. Dickey, J. M. & Paskin, A. Computer simulation of the lattice dynamics of solids. *Phys. Rev.* **188**, 1407–1418 (1969).
13. Keyes, T. Instantaneous normal mode approach to liquid state dynamics. *J. Phys. Chem. A* **101**, 2921–2930 (1997).
14. Dunegan, H., Harris, D. & Tatro, C. Fracture analysis by use of acoustic emission. *Engineering Fracture Mechanics* **1**, 105–122 (1968).
15. Nair, A. & Cai, C. S. Acoustic emission monitoring of bridges: Review and case studies. *Engineering Structures* **32**, 1704–1714 (2010).
16. Paparo, G., Gregori, G. P., Coppa, U., de Ritis, R. & Taloni, A. Acoustic Emission (AE) as a diagnostic tool in geophysics. *Annals of Geophysics* **45**, 401–416 (2002).
17. Nasuno, S., Kudrolli, A. & Gollub, J. P. Friction in granular layers: Hysteresis and precursors. *Phys. Rev. Lett.* **79**, 949–952 (1997).
18. Garcimartín, A., Guarino, A., Bellon, L. & Ciliberto, S. Statistical Properties of Fracture Precursors. *Phys. Rev. Lett.* **79**, 3202–3205 (1997).

19. Johnson, P. A. *et al.* Acoustic emission and microslip precursors to stick-slip failure in sheared granular material. *Geophysical Research Letters* **40**, 5627–5631 (2013).
20. Owens, E. T. & Daniels, K. E. Sound propagation and force chains in granular materials. *Europhysics Letters* **94**, 54005 (2011).
21. Majmudar, T. S. & Behringer, R. P. Contact force measurements and stress-induced anisotropy in granular materials. *Nature* **435**, 1079–82 (2005).
22. Brodu, N., Dijksman, J. A. & Behringer, R. P. Spanning the scales of granular materials through microscopic force imaging. *Nature Communications* **6**, 6361 (2015).
23. Hurley, R., Hall, S., Andrade, J. & Wright, J. Quantifying Interparticle Forces and Heterogeneity in 3D Granular Materials. *Phys. Rev. Lett.* **117**, 098005 (2016).
24. Silbert, L. E., Liu, A. J. & Nagel, S. R. Vibrations and diverging length scales near the unjamming transition. *Phys. Rev. Lett.* **95**, 098301 (2005).
25. Manning, M. L. & Liu, A. J. Vibrational Modes Identify Soft Spots in a Sheared Disordered Packing. *Phys. Rev. Lett.* **107**, 108302 (2011).

Acknowledgments This work was supported by NSF Grant DMR-1206808 and the James S. McDonnell Foundation. We would like to thank Paul Johnson, Craig Maloney, Corey O’Hern and Eli Owens for helpful discussions, and Cross Automation for advice and technical assistance with our motion control needs.

Author Contributions T.A.B. built the experimental apparatus and performed the experiments. T.A.B. and K.E.D. provided analysis, interpreted the data and wrote the paper.

Competing Interests The authors declare that they have no competing financial interests.

Correspondence Correspondence and requests for materials should be addressed to Ted Brzinski (email: tbrzinski@haverford.edu).